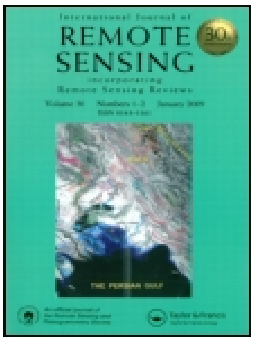

International Journal of Remote Sensing

ISSN: 0143-1161 (Print) 1366-5901 (Online) Journal homepage: http://www.tandfonline.com/loi/tres20

Segmentation and Tracking of Marine Cellular Clouds observed by Geostationary Satellites

Alisa Gufan, Yoav Lehahn, Erick Fredj, Colin Price, Rachel Kurchin & Ilan Koren

To cite this article: Alisa Gufan, Yoav Lehahn, Erick Fredj, Colin Price, Rachel Kurchin & Ilan Koren (2016) Segmentation and Tracking of Marine Cellular Clouds observed by Geostationary Satellites, International Journal of Remote Sensing, 37:5, 1055-1068, DOI: 10.1080/2150704X.2016.1142681

To link to this article: http://dx.doi.org/10.1080/2150704X.2016.1142681

Published online: 12 Feb 2016.

INTERNATIONAL JOURNAL OF REMOTE SENSING, 2016
VOL. 37, NO. 5, 1055–1068
http://dx.doi.org/10.1080/2150704X.2016.1142681

Taylor & Francis
Taylor & Francis Group

Segmentation and Tracking of Marine Cellular Clouds observed by Geostationary Satellites

Alisa Gufan[a,b], Yoav Lehahn[a], Erick Fredj[c,d], Colin Price[b], Rachel Kurchin[e] and Ilan Koren[a]

[a]Department of Earth and Planetary Sciences, Weizmann Institute of Science, Rehovot, Israel; [b]Department of Geosciences, Tel Aviv University, Ramat Aviv, Israel; [c]Department of Computer Sciences, The Jerusalem College of Technology, Jerusalem, Israel; [d]Department of Marine and Coastal Sciences Rutgers, The State University of New Jersey, New Brunswick, NJ, USA; [e]Department of Materials Science and Engineering, Massachusetts Institute of Technology, Cambridge, MA, USA

ABSTRACT

Marine stratocumulus (MSC) are shallow marine boundary layer clouds that have a significant cooling contribution to the Earth's radiative balance. The amplitude of this cooling effect strongly depends on the properties of closed and open cells comprising MSC cloud fields. Systematic study of the underlying processes associated with cloud cell properties requires accurate and reliable cell characterization. Here we propose a method for cell segmentation of MSC clouds as observed from geostationary satellite images. The method, which is based on watershed transformation, is found to be highly efficient in segmentation of both open and closed MSC scenes. Application of the suggested methodology over a Lagrangian framework that track the clouds as they are advected by the wind and comparison of the results between pairs of consecutive images indicate that the resulted segmentation is robust and consistent. The methodology developed in this work opens the way to systematic investigation of spatiotemporal changes in MSC cloud field properties, which will improve our understanding of MSC clouds and their role in regulating Earth's radiative budget.

ARTICLE HISTORY
Received 20 September 2015
Accepted 7 January 2016

1. Introduction

Accounting for more than half of Earth's albedo (Trenberth, Fasullo, and Kiehl 2009), clouds play a major role in the climate system. Yet, because of their dynamic and microphysical complexity, they are the least understood climate parameter (Forster et al. 2007). Of special importance are marine stratocumulus (MSC) clouds, which form large decks that cover millions of square kilometres over the subtropical and mid-latitude oceans (Figure 1a) (Feingold et al. 2010; Wood 2012; Koren and Feingold 2013; Goren and Rosenfeld 2014). By increasing Earth's shortwave albedo (as opposed to the dark oceans below the clouds), while radiating in the long wave at approximately the same temperature as the surface, these shallow marine boundary layer clouds have a significant cooling contribution to Earth's radiative balance (Hartmann and Doelling 1991). The net radiative forcing of MSC clouds is controlled by microphysical and

CONTACT Ilan Koren ilan.koren@weizmann.ac.il Department of Earth and Planetary Sciences, Weizmann Institute of Science, Rehovot 76100, Israel

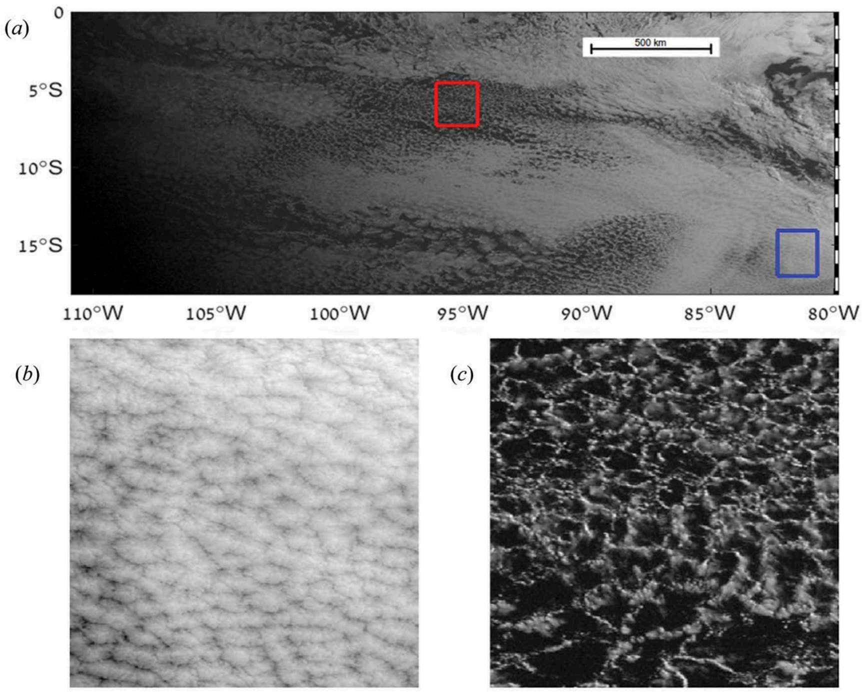

Figure 1. Satellite images of marine stratocumulus (MSC) clouds over the south-eastern Pacific Ocean from NOAA satellite GOES-13. (a) MSC cloud field from 4 August 2011. Note the co-existence of closed cells (fully covered with high albedo cloud field; e.g. region outlined by blue rectangle) and open cells (low cloud cover with low albedo cloud fields; e.g. region outlined by red rectangle) regions. (b, c) Magnification of the regions of interest (ROIs) outlined by the blue and red rectangles, respectively. The morphological characteristics of the two ROIs are investigated throughout the text.

morphological properties (Muhlbauer, McCoy, and Wood 2014), which depend on different environmental factors, such as aerosols concentrations (Rosenfeld, Kaufman, and Koren 2006; Bar-Or, Gildor, and Erlick 2011; Lehahn et al. 2011; Goren and Rosenfeld 2012) and meteorological conditions (Kazil et al. 2014).

MSC clouds were shown to form a classical bifurcated system with two dynamical states: open and closed cells (Stevens et al. 2005; Rosenfeld, Kaufman, and Koren 2006; Feingold et al. 2010; Koren and Feingold 2011; Wood 2012). The two states are clearly observed in satellite images of MSC cloud fields (Figure 1b and c). In general, closed cell clouds form when air rises at the middle of the cell and sinks along the walls resulting in continuous, highly covered and therefore highly reflective cloud fields (Figure 1b). The opposite accounts for open cells; where the clouds form along the cell's walls, resulting in much lower coverage and reflectivity (Figure 1c). Closed cells were shown to have preference to cold water and shallow marine atmospheric boundary layer (MBL) conditions that can be found near the coasts of eastern subtropical oceans. As the water warms and the MBL thickens with distance from the coastline, a transition to larger closed cells followed by a formation of open cells and later trade cumulus clouds takes place (Wood and Hartmann 2006; Muhlbauer, McCoy, and Wood 2014).

As the cloud field's albedo strongly depends on the cloud cell properties, there is a great need to understand how these properties change in response to variations in the environmental conditions. A major source of data comes from geostationary satellites that provide long-term information on cloud morphological and microphysical properties (Minnis, Smith, and Young 2001). Systematic application of these data for studying the underlying processes associated with cloud cell properties requires accurate and reliable cell characterization. Here we aim at the first and most critical stage of this important mission, and suggest a method for cell segmentation in MSC as observed in satellite images.

Our study follows previous attempts to develop numerical techniques for systematic characterization of cell patterns in MSC. Gryschka, Witha, and Etling (2008) used a pattern recognition algorithm that is based on delineation of ellipses around MSC clouds. The resulting cloud's equivalent radius distribution was fitted as a power law both in satellite and model data. This method was applied only to cases of closed cell MSC fields. In addition, the inherent limitation to cover a two-dimensional space with ellipses reduces the efficiency of the methods in cases of very dense fields of closed cell MSC, which are polygonal in nature. Wood and Hartmann (2006) used frequency analysis of satellite-derived liquid water path to characterize MSC field properties, namely cloud size, cell size and convection type. While providing useful information on the properties of the cloud field as a whole, the method does not provide any information on the spatial characteristic of individual cells. Recently, it was shown that studying the time evolution of individual cells is an important stage towards understanding the processes that control MSC in general and in particular setups and transitions between states (Feingold et al. 2010; Koren and Feingold 2011, 2013).

Cloud cell segmentation is not a well-defined problem because different applications may require different segmentation types. Specifically since clouds tend to have a fractal nature (Cahalan et al. 1994; Yamaguchi and Feingold 2013) a cell of large scale (in the order of tens of kilometres) may consist of finer-scale structures. This problem is more profound in the case of closed cells, where each main (large scale) cell can be subdivided to many smaller convective units.

Here we report on a segmentation method developed for MSC cloud cells that is tuned to be sensitive to the large-scale cells and as importantly is tuned to be robust and consistent. To do so we developed a watershed-based morphological transformation (WMT), which is based on interpretation of a grey scale image as a topographic surface, with the grey scale levels corresponding to topographic height (Beucher and Lantuéjoul 1979). Accordingly, the segmentation is performed by identifying watershed regions. WMT was previously applied for characterizing spatial properties of clouds. González et al. (2012) used segmentation based on WMT as a first step in an automatic technique for cloud detection and classification. Lakshmanan, Hondl, and Rabin (2009) used WMT for identifying storms in satellite and radar images. In addition, segmentation by WMT is commonly used for many other applications, including biology (Karvelis, Likas, and Fotiadis 2010), medical imagery (Grau et al. 2004), face recognition (Brethes et al. 2004), remote sensing interpretation (Li et al. 2010) and geophysics (Roueff et al. 2004).

2. Satellite data

Images of MSC clouds fields are derived from band 1 (visual range, 550–750 nm) of the Geostationary Operational Environmental Satellite (GOES-13, http://goes.gsfc.nasa.gov/) IMAGER radiometer owned and operated by the National Oceanic and Atmospheric

Administration (NOAA). The spatial resolution is 1 km in nadir, with one image acquired every 30 minutes during daytime.

In this study we used the dataset for an area located between 80–110° W and 0–18° S, which is part of the 'Northern Hemisphere Extended' GOES-EAST Imager Scan Sectors in Routine Mode (http://www.nsof.class.noaa.gov/release/data_available/goes/index.htm). This region covers the largest and most persistent subtropical MSC deck, over the south-eastern Pacific Ocean (Klein and Hartmann 1993). The data are downloaded from the Comprehensive Large Array-data Stewardship System (CLASS) (http://www.class.ngdc.noaa.gov/saa/products/catSearch). The segmentation was performed over 300 km × 300 km scenes that were manually chosen based on cloud morphology.

3. Step-by-step image segmentation

As introduced in Section 1, the segmentation of open and closed MSC cells is performed by applying the WMT, where the segmentation is associated with ridges of local grey-scale maxima. This approach is ideal for delineating boundaries of open cells, in which narrow regions of high grey-scale levels (i.e. the clouds at the cell edges) form *n*-torus with distinct regions of low grey-scale level at their centre (i.e. the ocean below, Figure 1c – open cells) (Koren and Feingold 2013).

In the case of closed cell MSC, where local grey-scale maxima are found at the *n*-torus centres (Figure 1b), the normalized cell image I is first transformed to its negative image:

$$I_1(x,y) = \begin{cases} I(x,y) & \text{for open cells} \\ 1 - I(x,y) & \text{for closed cells} \end{cases} \tag{1}$$

where x and y are the coordinates and $I_1(x,y)$ is image after the transformation in case of closed cells and identical to I for open cells.

After this stage closed cells border pixels have greater values than inner cell pixels, and the resultant images have, in principle, similar characteristics as open cell images. Following that, unless stated otherwise, the segmentation algorithm is similar for both open and closed cells, and consists of three major steps (Figure 2a): (i) histogram equalization and low pass filtering; (ii) morphological transformation preprocessing; and (iii) WMT. The three steps are demonstrated for the closed and open cell scenes outlined in Figure 1 (Figure 2b–e, lower and upper panels, respectively).

3.1. *Histogram equalization and low pass filtering*

This stage is meant to focus on the dynamical range which contains most of the information relevant to our study. The resulting images are shown in Figure 2c. Modification of the image contrast is done using adaptive histogram equalizing and mapping the brightness distributions to a fixed one (in our case Rayleigh distribution). Based on examination of a large number (>~500) of satellite images, we learned that the typical borders of closed cells are characterized by normalized reflectance levels of between 0.00 and 0.20, whereas the core of the closed cells is always larger than 0.72. Therefore the values in the ranges 0.00–0.20 and 0.72–1.00 were truncated to 0 and 1, respectively. In the case of open cells, which are characterized by much stronger

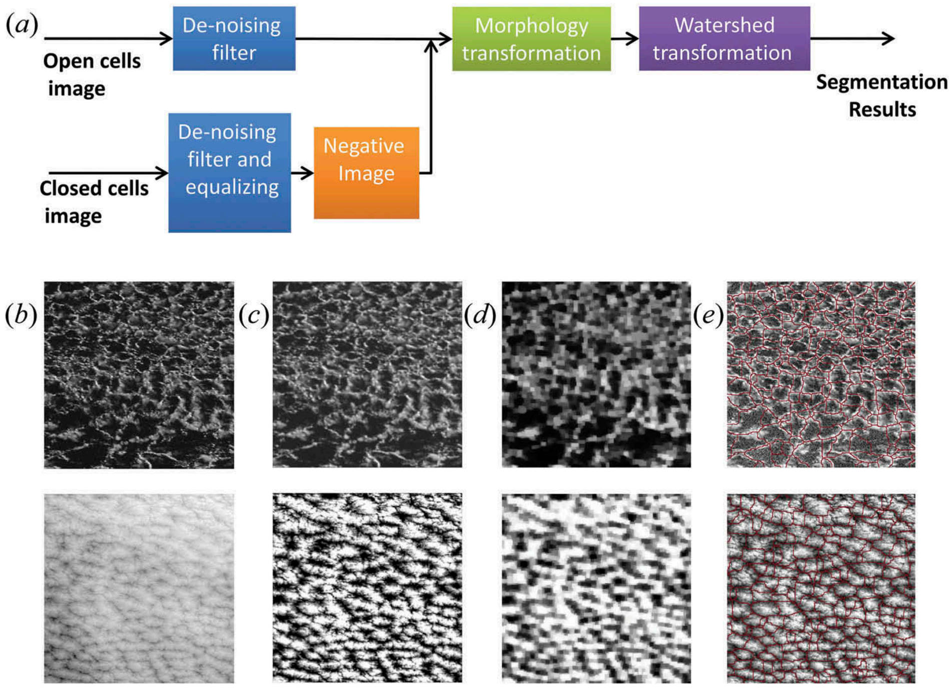

Figure 2. Steps of the segmentation algorithm. (a) A scheme describing different steps of the algorithm. (b–e) Step-by-step segmentation of closed (lower panels) and open (upper panels) MSC cloud cells, as follows: (b) original satellite images; (c) image after filtering and histogram equalizing; (d) image after morphological transformation; and (e) resulting segmentation (purple lines) superimposed on the original image. The process is applied on the two regions of interest outlined in Figure 1.

contrast, histogram equalizing is redundant and is not performed. Following the adaptive histogram equalizing, we filter high-frequency noise using a Gaussian low pass filter (diameter equals 30 km and standard deviation equals 0.5). This step is applied on both open and closed cell images.

3.2. *Morphological transformation preprocessing*

A common problem in applying WMT is over-segmentation (Beucher and Meyer 1992; Beucher 1994; Ng et al. 2006), which in our case would result in a very large number of small cells. In order to avoid this problem while preserving significant structural elements, we perform mathematical morphological transformations (Haralick, Sternberg, and Zhuang 1987; Maragos and Schafer 1987a, 1987b) that smooth the image and remove irrelevant local extreme points (Figure 2d). The transformation consists of morphological closing (i.e. image dilation followed by image erosion) and morphological opening (i.e. image erosion followed by image dilation) operators that are applied sequentially with the same structuring element.

The main parameter of these transformations is the structuring element. To estimate the optimal structure element diameter we used a set of training images that were segmented manually by us and by our algorithm, and compared number of detected cells. We tested structure element diameters of between3 and 17 km. In agreement with the reported MSC cell characteristic scale of 10 km or more (Feingold et al. 2010; Koren and Feingold 2013) the acceptable results were achieved using structuring elements in the diameter range of 5–9 km. Application of smaller structuring elements resulted in over segmentation, while application of bigger structuring elements missed important cloud structures. For consistency the structuring element is defined here to be a disc with a diameter of 7 km, reducing the likelihood for contribution of small structures that are on the limit of the satellite resolution.

3.3. *Watershed transformation*

The final stage in the cell segmentation process is the watershed transformation (WST), which is a morphological method for image segmentation (Beucher and Lantuéjoul 1979) (Figure 2e). Intuitively it can be described as attributing the reflectance (or grey-level values) of each pixel to the pixels elevation. So any 2D image is interpreted as a 3D surface P, with the grey-level values scaled as the vertical coordinate:

$$P = \{(x,y,I_1(x,y))\} \tag{2}$$

where x and y are the coordinates and $I_1(x,y)$ is the grey level of the input satellite image (after the above processing stages). Taking a topographic surface as a reference, segmentation borders are defined as the surface's watershed lines (Lin et al. 2006).

4. Sequence segmentation in a Lagrangian framework

Next, we evaluate the robustness of our WMT method, namely its ability to provide consistent segmentation of closed and open cellular cloud patterns. This is done by comparing segmentation results from a sequence of consecutive images of the same cloud field. The approach is based on the assumption that the characteristic lifetime of a cloud cell is much longer than the 30 minutes time differences between two consecutive satellite images (Koren and Feingold 2013). Therefore the cloud field maintains most of its morphological features and the WMT should result in similar segmentation patterns when applied on consecutive cloud field images.

Analysis of the method's robustness by comparing the WMT results for sequences of images requires very accurate tracking of the segmented region as it is advected by the wind. For that we apply the Lagrangian tracking methodology recently developed by Koren and Feingold (2013). The method for finding the displacement that yields the best similarities between two consecutive cloud field images is based on minimizing the absolute Euclidean distance (L_2), between a matrix defined as the steepness matrix (**S**), which is composed of the Euclidean sum of the gradients along the x and the y coordinates:

$$S_t(x,y) = \sqrt{\left(\frac{\partial I_{1t}(x,y)}{\partial x}\right)^2 + \left(\frac{\partial I(x,y)_{1t}}{\partial y}\right)^2} \tag{3}$$

where I_{1t} is the satellite-processed image at a time t, and $S_t(x, y)$ is the steepness matrix element at time t and x, y coordinates.

Next, the optimal displacement (a_o, b_o) is found by minimizing the Euclidean distance between each pair of consecutive steepness matrix as following:

$$(a_o, b_o) = \text{argmin}\{\| S_t(x, y), S_{t+1}(x \pm a\Delta x, y \pm b\Delta y)\|_2\} \tag{4}$$

where a and b are the displacements and Δx and Δy are the pixel resolution along the x and y axes, respectively.

To save calculation time the displacement was restricted to be smaller than 30 km. Distance of 30 km in a 30 minutes time interval corresponds to an advection speed of more than 16 m s^{-1}, which marks the very high end of surface winds in MSC regions. As in Koren and Feingold (2013) this tracking method shows single, well-defined results for all examined cases.

Figures 3 and 4 show the evolution in time of the two scenes discussed earlier (from 4 August 2011 over the south-eastern Pacific Ocean; Figures 1 and 2). During a 4.5 hours period (12:45–17:15), in both closed (Figure 3) and open (Figure 4) cell scenes, the sequence images are relatively similar. On longer time scales the two cellular structure types differ. While closed cells maintain distinct coherent structures that can, in some cases, be tracked for a few hours (Koren and Feingold 2013 – see, e.g. cell segmented by yellow contour in Figure 3), open cells have a shorter lifetime (order of 2 hours) and tend to oscillate between cloud to cloud-free states (Feingold et al. 2010) and therefore the image similarity degraded significantly for time differences larger than the characteristic cell timescale.

4.1. *Quantitative comparison of cellular cloud segmentation*

Quantification of the differences in cellular segmentation in different images is based on calculation of Rand index (RI, Rand 1971). This index follows the notion that two pixels of a segmented image (with zero-width borders) can be found in one of two topological conditions: part of one segment or between two different segments. Accordingly, RI values are defined as the proportion of possible pixel pairs that are in equivalent topological condition in both segmentations. RI between identical segmentations equals 1, and the RI is 0 when first segmentation results in only one segment while the number of segments in the second segmentation equals to the number of pixels in the original image. Formally, RI is defined as follows:

$$\text{RI} = \frac{a + c}{a + b + c + d} = \frac{a + c}{\binom{n}{2}} \tag{5}$$

where n is the total number of pixels in the image; a, the number of pixel pairs that are in the same segment in both segmentation; b, the number of pixel pairs that are in the same segment in the first segmentation and in different segments in the second segmentation; c, the number of pixel pairs that are in different segments in both segmentations; and d, the number of pixel pairs that are in different segments in the first segmentation and are in the same segment in second segmentation, and

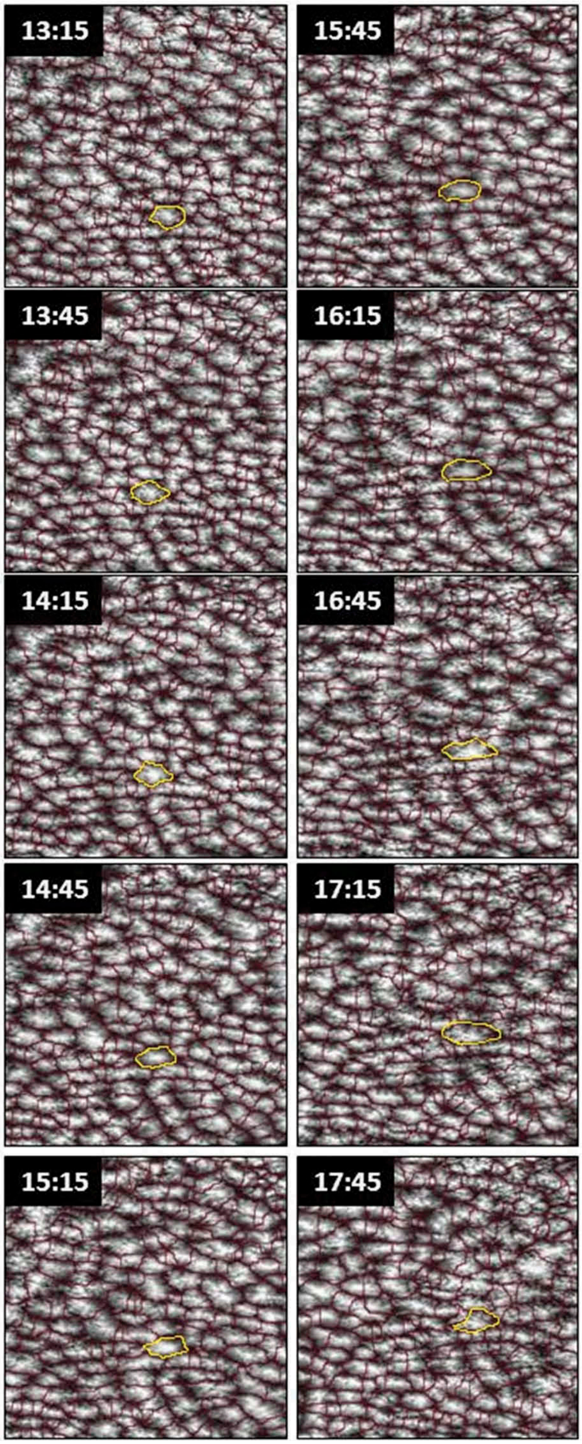

Figure 3. Segmentation of the closed cells region of interest (blue rectangle in Figure 1) as it evolves during the day (4 August 2011). Yellow contour highlights one of the cells that was tracked throughout the 4.5 hours analysis.

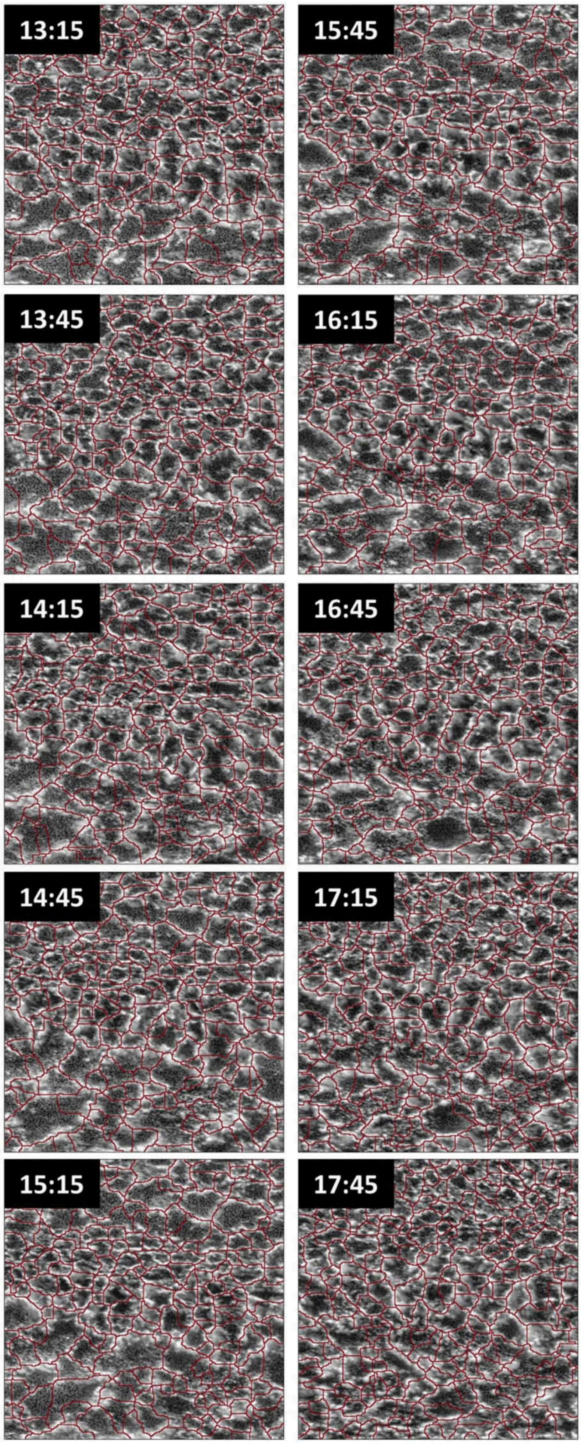

Figure 4. As Figure 3 but for the open cells region of interest. Area enclosed by the red rectangle in Figure 1.

$$\binom{n}{2} = \frac{n(n-1)}{2} \text{is the total number of possible pairs.} \tag{6}$$

A problem with the RI is that the expected value for two random clusters is not zero. We therefor adopt the adjusted Rand index (ARI, Hubert and Arabie 1985), to avoid or bypass the problem. Application of this comparison method requires associating each pixel in the image to a specific segment (in our watershed segmentation the lines are not considered part of segments). Thus, before calculating the ARI parameter, we resize the segmentation results and delete the borders by a nearest-neighbour interpolation (Parker, Kenyon, and Troxel 1983).

The RI method is most commonly used for comparison between different clustering methods as applied on a single image (Rand 1971; Arbelaez et al. 2011). In contrast, here we use ARI calculation to estimate the consistency of a single segmentation method when applied over a series of images describing a time-varying cloud field that is tracked in a Lagrangian manner. When calculated for a series of sequential images (with 30 minutes time difference), the ARI maintains relatively high values of between 0.83 and 0.94, and between 0.77 and 0.87 for closed and open cell scenes, respectively (black thick line in Figure 5a and b). This is in agreement with the relatively small changes in cloud patterns and associated segmentation revealed in qualitative comparison between the images in the images (Figures 3 and 4).

To test the robustness of the segmentation methodology, and its applicability for systematic study of MSC cloud fields, we perform a similar analysis (i.e. calculation of ARI for segmentation of sequential images) for 10 scenes of closed and open cells MSC cloud over the same region. We chose scenes that are (1) distinctly characterized as either closed or open; and (2) tracked over a period of a few hours (in order to allow long-term comparison using ARI). Overall, for all closed and open cellular cloud scenes the WMT method provides consistent segmentation. This is emphasized by ARI, which maintains relatively high values for evolving fields of closed (between 0.71 and 0.94, Figure 5a) and open (between 0.74 and 0.94, Figure 5b) cloud cells.

5. Discussion

We use WMT to segment open and closed cells in fields of MSC clouds. Application of the WMT over a Lagrangian framework that tracks the clouds as they are advected by the wind, and comparison of the results between pairs of images taken at short time intervals, indicate that the method provides a robust and consistent segmentation of open and closed cells MSC clouds.

A major advancement in applying the watershed methods for segmentation of MSC cell patterns, which are very heterogeneous in shape and size (see, e.g. Figure 1), is the adaptive form of the resulting segments. Importantly, this allows capturing the compact area coverage by the cells, which is characteristic to both open and closed cell patterns. This is not possible in various popular shape-based pattern recognition methods as the ellipse recognition (Mai et al. 2008), which is constrained to a limited range of spatial segmentation forms. However, while being highly efficient in segmenting cellular patterns in MSC clouds, currently the methodology developed in this work is tuned to scenes with well-defined cell state (closed or open).

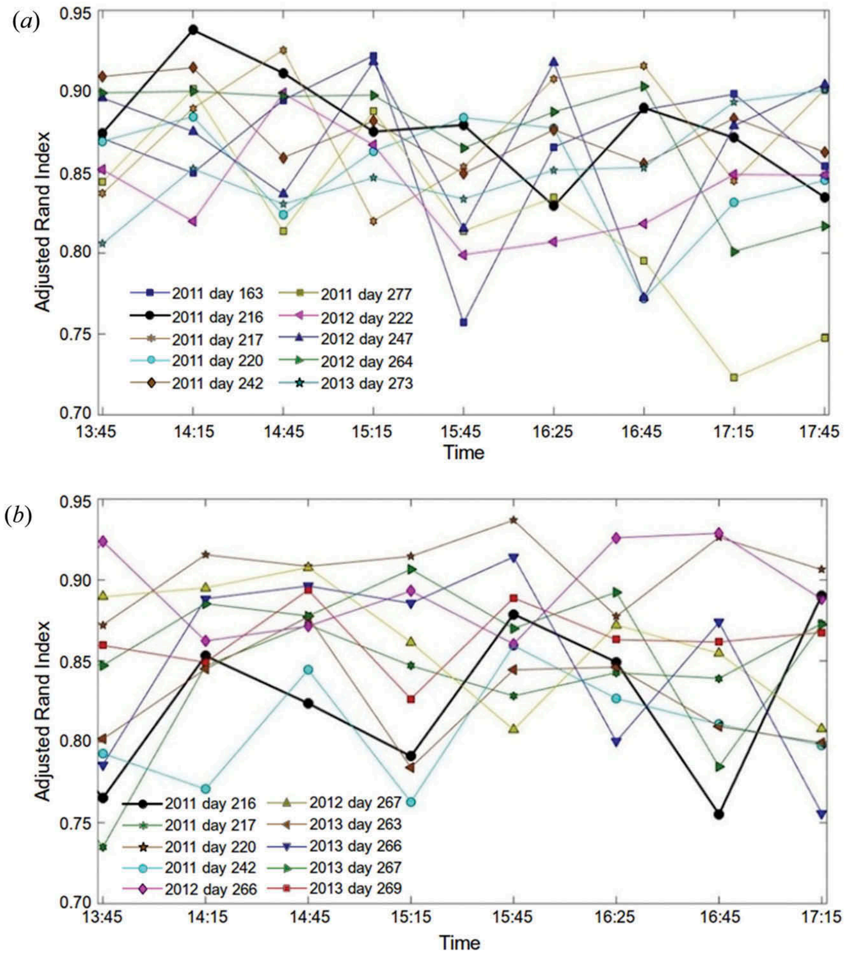

Figure 5. Evaluation of the method consistency. Values of adjusted Rand index (ARI) between sequential images of time-evolving (a) closed cells and (b) open cells scenes from different days. Black solid lines represent the ARI values for the closed and open cell scenes discussed in the text (Figure 3 and 4, respectively).

The ability of the WMT methodology to provide consistent and robust segmentation of MSC cellular cloud patterns is further emphasized by the high values of ARI between pairs of sequential closed and open cell scenes (Figure 5). In addition, the relatively high ARI values support the underlying assumption that for a limited period of 30 minutes (the time interval between two consecutive images), the MSC field is likely to conserve its cellular structure. In addition, our analysis reveals distinct differences between closed and open cell patterns. For example, while open cells have a relatively short lifetime, closed cells are relatively stable and, in some cases, can be tracked over periods of several hours.

By allowing accurate segmentation of cellular cloud patterns, application of the WMT methodology opens the way for systematic investigation of spatiotemporal changes in MSC cloud field properties, and of their dependency on various environmental factors. This will have important contribution to our understanding of MSC clouds and of their role in regulating Earth's radiative budget.

Disclosure statement

No potential conflict of interest was reported by the authors.

Funding

The research leading to these results has received funding from the European Research Council under the European Union’s Seventh Framework Programme [grant number FP7/2007–2013]/ERC Grant (CAPRI) [grant number 306965].

References

Arbelaez, P., M. Maire, C. Fowlkes, and J. Malik. 2011. “Contour Detection and Hierarchical Image Segmentation.” *IEEE Transactions on Pattern Analysis and Machine Intelligence* 33 (5): 898–916. doi:10.1109/TPAMI.2010.161.

Bar-Or, R., H. Gildor, and C. Erlick. 2011. “The Aerosol-Bénard Cell Effect on Marine Stratocumulus Clouds and Its Contribution to Glacial-Interglacial Cycles.” *Journal of Geophysical Research* 116. doi:10.1029/2010JD014470.

Beucher, S. 1994. “Watershed, Hierarchical Segmentation and Waterfall Algorithm.” In *Mathematical Morphology and its Applications to Image Processing*, edited by J. Serra and P. Soille. 69–76. Springer.

Beucher, S., and C. Lantuéjoul. 1979. “Use of Watersheds in Contour Detection.” In International Workshop on Image Processing, Real-time Edge and Motion Detection.

Beucher, S., and F. Meyer. 1992. “The Morphological Approach to Segmentation: The Watershed Transformation.” In *Mathematical Morphology in Image Processing*, edited by E. R. Dougherty, 433. New York: Marcel Dekker Incorporated.

Brethes, L., P. Menezes, F. Lerasle, and J. Hayet. 2004. “Face Tracking and Hand Gesture Recognition for Human-Robot Interaction.” In *Proceedings of the 2004 IEEE International Conference on Robotics and Automation*, 1901–1906. New Orleans, LA: IEEE.

Cahalan, R. F., W. Ridgway, W. J. Wiscombe, T. L. Bell, and J. B. Snider. 1994. “The Albedo of Fractal Stratocumulus Clouds.” *Journal of the Atmospheric Sciences* 51 (16): 2434–2455. doi:10.1175/1520-0469(1994)051<2434:TAOFSC>2.0.CO;2.

Feingold, G., I. Koren, H. Wang, H. Xue, and W. A. Brewer. 2010. “Precipitation-Generated Oscillations in Open Cellular Cloud Fields.” *Nature* 466: 849–852. doi:10.1038/nature09314.

Forster, P., V. Ramaswamy, P. Artaxo, T. Berntsen, R. Betts, D. W. Fahey, J. Haywood, et al. 2007. “Changes in Atmospheric Constituents and in Radiative Forcing.” In *Climate Change 2007: The Physical Science Basis. Contribution of Working Group I to the Fourth Assessment Report of the Intergovernmental Panel on Climate Change*, edited by S. Solomon, D. Qin, M. Manning, Z. Chen, M. Marquis, K. B. Averyt, M. Tignor, and H. L. Miller. Cambridge: Cambridge University Press.

González, A., J. C. Pérez, J. Muñoz, Z. Méndez, and M. Armas. 2012. “Watershed Image Segmentation and Cloud Classification from Multispectral MSG-SEVIRI Imagery.” *Advances in Space Research* 49 (1): 135–142. doi:10.1016/j.asr.2011.09.023.

Goren, T., and D. Rosenfeld. 2012. “Satellite Observations of Ship Emission Induced Transitions from Broken to Closed Cell Marine Stratocumulus over Large Areas.” *Journal of Geophysical Research*. doi:117:10.1029/2012JD017981.

Goren, T., and D. Rosenfeld. 2014. “Decomposing Aerosol Cloud Radiative Effects into Cloud Cover, Liquid Water Path and Twomey Components in Marine Stratocumulus.” *Atmospheric Research* 138: 378–393. doi:10.1016/j.atmosres.2013.12.008.

Grau, V., A. Mewes, M. Alcaniz, R. Kikinis, and S. K. Warfield. 2004. “Improved Watershed Transform for Medical Image Segmentation Using Prior Information.” *IEEE Transactions on Medical Imaging* 23 (4): 447–458. doi:10.1109/TMI.2004.824224.

Gryschka, M., B. Witha, and D. Etling. 2008. “Scale Analysis of Convective Clouds.” *Meteorologische Zeitschrift* 17 (6): 785–791. doi:10.1127/0941-2948/2008/0345.

Haralick, R. M., S. R. Sternberg, and X. Zhuang. 1987. "Image Analysis Using Mathematical Morphology." *IEEE Transactions on Pattern Analysis and Machine Intelligence* PAMI-9: 532–550. doi:10.1109/TPAMI.1987.4767941.

Hartmann, D. L., and D. Doelling. 1991. "On the Net Radiative Effectiveness of Clouds." *Journal of Geophysical Research: Atmospheres* 96: 869–891. doi:10.1029/90JD02065.

Hubert, L., and P. Arabie. 1985. "Comparing Partitions." *Journal of Classification* 2 (1): 193–218. doi:10.1007/BF01908075.

Karvelis, P., A. Likas, and D. I. Fotiadis. 2010. "Identifying Touching and Overlapping Chromosomes Using the Watershed Transform and Gradient Paths." *Pattern Recognition Letters* 31 (16): 2474–2488. doi:10.1016/j.patrec.2010.08.002.

Kazil, J., G. Feingold, H. Wang, and T. Yamaguchi. 2014. "On the Interaction between Marine Boundary Layer Cellular Cloudiness and Surface Heat Fluxes." *Atmospheric Chemistry and Physics* 14 (1): 61–79. doi:10.5194/acp-14-61-2014.

Klein, S. A., and D. L. Hartmann. 1993. "The Seasonal Cycle of Low Stratiform Clouds." *Journal of Climate* 6 (8): 1587–1606. doi:10.1175/1520-0442(1993)006<1587:TSCOLS>2.0.CO;2.

Koren, I., and G. Feingold. 2011. "Aerosol-Cloud-Precipitation System as a Predator-Prey Problem." *Proceedings of the National Academy of Sciences* 108 (30): 12227–12232. doi:10.1073/pnas.1101777108.

Koren, I., and G. Feingold. 2013. "Adaptive Behavior of Marine Cellular Clouds." *Scientific Reports* 3. doi:10.1038/srep02507.

Lakshmanan, V., K. Hondl, and R. Rabin. 2009. "An Efficient, General-Purpose Technique for Identifying Storm Cells in Geospatial Images." *Journal of Atmospheric and Oceanic Technology* 26 (3): 523–537. doi:10.1175/2008JTECHA1153.1.

Lehahn, Y., I. Koren, O. Altaratz, and A. B. Kostinski. 2011. "Effect of Coarse Marine Aerosols on Stratocumulus Clouds." *Geophysical Research Letters* 38. doi:10.1029/2011GL048504.

Li, D., G. Zhang, Z. Wu, and L. Yi. 2010. "An Edge Embedded Marker-Based Watershed Algorithm for High Spatial Resolution Remote Sensing Image Segmentation." *IEEE Transactions on Image Processing* 19 (10): 2781–2787. doi:10.1109/TIP.2010.2049528.

Lin, Y.-C., Y.-P. Tsai, Y.-P. Hung, and Z.-C. Shih. 2006. "Comparison between Immersion-Based and Toboggan-Based Watershed Image Segmentation." *IEEE Transactions on Image Processing* 15 (3): 632–640. doi:10.1109/TIP.2005.860996.

Mai, F., Y. Hung, H. Zhong, and W. Sze. 2008. "A Hierarchical Approach for Fast and Robust Ellipse Extraction." *Pattern Recognition* 41 (8): 2512–2524. doi:10.1016/j.patcog.2008.01.027.

Maragos, P., and R. W. Schafer. 1987a. "Morphological Filters-Part I: Their Set-Theoretic Analysis and Relations to Linear Shift-Invariant Filters." *IEEE Transactions on Acoustics, Speech, and Signal Processing* 35 (8): 1153–1169. doi:10.1109/TASSP.1987.1165259.

Maragos, P., and R. W. Schafer. 1987b. "Morphological Filters-Part II: Their Relations to Median, Order-Statistic, and Stack Filters." *IEEE Transactions on Acoustics, Speech, and Signal Processing* 35 (8): 1170–1184. doi:10.1109/TASSP.1987.1165254.

Minnis, P., W. Smith Jr, and D. Young. 2001. "Cloud Macro-And Microphysical Properties Derived from GOES over the ARM SGP Domain." In Eleventh ARM Science Team Meeting Proceedings.

Muhlbauer, A., I. McCoy, and R. Wood. 2014. "Climatology of Stratocumulus Cloud Morphologies: Microphysical Properties and Radiative Effects." *Atmospheric Chemistry and Physics* 14 (13): 6695–6716. doi:10.5194/acp-14-6695-2014.

Ng, H., S. Ong, K. Foong, P. Goh, and W. Nowinski. 2006. "Medical Image Segmentation Using K-Means Clustering and Improved Watershed Algorithm." In *2006 IEEE Southwest Symposium on Image Analysis and Interpretation*, 61–65. New York: IEEE.

Parker, J. A., R. V. Kenyon, and D. Troxel. 1983. "Comparison of Interpolating Methods for Image Resampling." *IEEE Transactions on Medical Imaging* 2 (1): 31–39. doi:10.1109/TMI.1983.4307610.

Rand, W. M. 1971. "Objective Criteria for the Evaluation of Clustering Methods." *Journal of the American Statistical Association* 66 (336): 846–850. doi:10.1080/01621459.1971.10482356.

Rosenfeld, D., Y. Kaufman, and I. Koren. 2006. "Switching Cloud Cover and Dynamical Regimes from Open to Closed Benard Cells in Response to the Suppression of Precipitation by Aerosols." *Atmospheric Chemistry and Physics* 6 (9): 2503–2511. doi:10.5194/acp-6-2503-2006.

Roueff, A., J. Chanussot, J. I. Mars, and M.-Q. Nguyen. 2004. "Unsupervised Separation of Seismic Waves Using the Watershed Algorithm on Time-Scale Images." *Geophysical Prospecting* 52 (4): 287–300. doi:10.1111/gpr.2004.52.issue-4.

Stevens, B., G. Vali, K. Comstock, R. Wood, C. van Zanten, P. H. Austin, C. S. Bretherton, and D. H. Lenschow. 2005. "Pockets of Open Cells and Drizzle in Marine Stratocumulus." *Bulletin of the American Meteorological Society* 86: 51–57. doi:10.1175/BAMS-86-1-51.

Trenberth, K. E., J. T. Fasullo, and J. Kiehl. 2009. "Earth's Global Energy Budget." *Bulletin of the American Meteorological Society* 90 (3): 311–323. doi:10.1175/2008BAMS2634.1.

Wood, R. 2012. "Stratocumulus Clouds." *Monthly Weather Review* 140 (8): 2373–2423. doi:10.1175/MWR-D-11-00121.1.

Wood, R., and D. L. Hartmann. 2006. "Spatial Variability of Liquid Water Path in Marine Low Cloud: The Importance of Mesoscale Cellular Convection." *Journal of Climate* 19 (9): 1748–1764. doi:10.1175/JCLI3702.1.

Yamaguchi, T., and G. Feingold. 2013. "On the Size Distribution of Cloud Holes in Stratocumulus and Their Relationship to Cloud-Top Entrainment." *Geophysical Research Letters* 40 (10): 2450–2454. doi:10.1002/grl.50442.